RSC Advances

RSC Advances

www.rsc.org/advances

ROYAL SOCIETY OF CHEMISTRY

www.rsc.org/advances

Journal Name

ARTICLE

Fe₃O₄ and paclitaxel loaded emulsion with charge-conversional surface for tumor MRI and therapy

Min Xu, Baoru Yin, Chunyang Li, Ping Yao*

In this study, Fe_3O_4 magnetic nanoparticles and paclitaxel loaded oil in water emulsion was fabricated for tumor-targeted chemotherapy, MRI and near-infrared photothermal therapy. Amphiphilic glycol chitosan-cholic acid conjugate (GCCA) was synthesized by amidation reaction and bovine serum albumin-dextran conjugate (BD) was produced by Maillard reaction. BD/GCCA electrostatic complex was used as a complex emulsifier to produce Fe_3O_4 and paclitaxel loaded emulsion by high pressure homogenization. The emulsion possesses an average droplet size of about 250 nm and a transversal R_2 relaxation rate of 326 $mM^{-1}s^{-1}$. The droplets are stable at physiological condition due to the dextran and glycol chitosan surface. The droplet surfaces are negatively charged at pH 7.4 and positively charged at pH 6.5. The droplets can be effectively accumulated at tumor site by attaching a small magnet to tumor and the pH sensitive charge-conversional surfaces may promote the tumorous cellular uptake of the droplets. *In vivo* investigation verified that the emulsion, administrated via tail vein and guided by an external magnetic field, significantly enhanced the anti-tumor efficacy and reduced the toxicity of paclitaxel as well as improved tumor contrast effect in T_2-weighted MRI. More importantly, after intratumoral injection of the emulsion and near-infrared laser irradiation, H22 solid tumors were completely eliminated.

1 Introduction

Magnetic nanoparticles (MNPs) have received tremendous attention in cancer treatment researches.[1] MNPs can be used as MRI contrast agents for tumor diagnosis,[2,3] and drug loaded MNPs can be directly accumulated at tumor site without special receptor recognition by manipulating external magnetic field.[4,5] In addition, MNPs possess good photothermal converting efficiency under near-infrared (NIR) laser irradiation, which can be used for photothermal ablation of tumors.[6] By combining MRI diagnosis with chemotherapy and phototherapy or magnetic hyperthermia together, multifunctional drug and MNPs loaded nanocarriers exhibit better effects on cancer treatment.[7-9] For instance, Shen *et al*. fabricated carboxymethyl chitosan (CMCTS) coated Fe_3O_4 particles.[10] By attaching a magnet to the tumor, Fe_3O_4@CMCTS particles accumulated in the tumor after intravenous injection. After being exposed to 808 nm laser, the tumors in Fe_3O_4@CMCTS-injected mice were completely destroyed. Zhou *et al* prepared multifunctional PEGylated $Fe@Fe_3O_4$ nanoparticles with triple functions of MRI, magnetic targeting, and NIR photothermal therapy.[11] These studies demonstrated that multifunctional MNPs could completely destroy tumors,

which are a promising approach to tumor therapy.

It was reported that approximately 40% of potential new drugs identified by the pharmaceutical companies are restricted in clinical translations due to their poor water solubility, low bioavailability as well as low absorption.[12] Various drug delivery nanocarriers, such as emulsions, liposomes, micelles and nanoparticles have been developed to improve the uptake of hydrophobic drugs.[13-15] Among various carriers, oil in water emulsions have attracted particular attention because of their remarkable advantages such as high loading efficiency and good bioavailability for hydrophobic drugs.[16] Furthermore, nano-sized emulsion can be easily produced by high pressure homogenization, a large-scale producible and reproducible emulsification method.[17,18] Natural proteins containing hydrophilic and hydrophobic residues in their primary structures are widely used as emulsifiers.[19] For example, albumin vehicles prepared by emulsification were already used for delivery of hydrophobic drugs in the 1970s.[20] Albumin-bound paclitaxel (PTX) nanoparticles formulation prepared by emulsification was approved by FDA in 2005.[21] However, protein emulsions are usually unstable and sensitive to temperature, pH and ionic strength.[22] Protein-polysaccharide emulsions, in which hydrophilic polysaccharide locates on the oil droplet surfaces, have better stability.[19,23] Previously, we used bovine serum albumin-dextran conjugate (BD) as an emulsifier to prepare PTX loaded emulsion.[24] Our *in vivo* study demonstrated that the emulsion significantly prolonged the life time of tumor bearing mice. In this study, we used oil in water emulsion to

State Key Laboratory of Molecular Engineering of Polymers, Collaborative Innovation Center of Polymers and Polymer Composite Materials, Department of Macromolecular Science, Fudan University, Shanghai 200433, China
*Correspondence to Ping Yao. E-mail: yaoping@fudan.edu.cn; Phone: 86-21 65642964; Fax: 86-21-65640293

COMMUNICATION

synchronously load hydrophobic anticancer drug PTX and Fe_3O_4 MNPs to enhance the anti-tumor efficacy.

Positively charged nanocarriers can facilitate the cell internalization via electrostatic interaction with negatively charged cell membrane.[25,26] However, the positive surfaces also lead to rapid clearance of the carriers by macrophages, which decrease the blood circulation time of the carriers.[27] Considering the mildly acidic extracellular pH (around 6.5) in most tumor tissues,[28] the nanocarriers with charge-conversional surfaces, which change their surface charges from negative or neutral at pH 7.4 to positive at pH 6.5, can simultaneously improve the tumorous cellular uptake and prolong the blood circulation time. Glycol chitosan (GCS) is a water-soluble and biocompatible chitosan derivative.[29] GCS carries positive charges at acidic pH and the positive charges decrease gradually with the increase of solution pH because of the deprotonation of the amine groups. In this study, amphiphilic glycol chitosan-cholic acid (GCCA) conjugate was synthesized. We used GCCA and BD electrostatic complex as a complex emulsifier to produce Fe_3O_4 MNPs and PTX loaded emulsion (Fe_3O_4/PTX@BD/GCCA) whose droplets have pH sensitive charge-conversional surfaces. The fabrication approach and structure of Fe_3O_4/PTX@BD/GCCA emulsion are illustrated in Scheme 1. The approach is an effective and facile one. Fe_3O_4/PTX@BD/GCCA emulsion possesses MRI, magnetic targeting, chemotherapy and NIR photothermal therapy functions. *In vivo* investigations demonstrated that Fe_3O_4/PTX@BD/GCCA emulsion is a promising system for tumor diagnosis and therapy.

2 Experimental

2.1 Materials

Bovine serum albumin (BSA, fraction V, 99%) and dextran (10 kDa) were supplied by Sangon Biotech Shanghai Co., Ltd. Medium chain triglyceride (MCT) for injection was purchased from Avic (Tieling) Pharmaceutical Co., Ltd. Paclitaxel (PTX) was from Jiangsu Yew Pharmaceutical Co., Ltd. Glycol chitosan (GCS, 82 kDa) and potassium poly(vinyl sulfate) solution were from Wako Pure Chemical Industries, Ltd. Toluidine blue was from J&K Scientific Ltd. N-hydroxysuccinimide (NHS, 99%) and 1-ethyl-3-(3-dimethylaminopropyl) carbodiimide hydrochloride (EDC, 99%) were from Sigma-Aldrich. Cholic acid (CA, 98%) was supplied by Bio Basic Inc. Dulbecco's modified Eagle's medium (DMEM) cell culture medium and fetal bovine serum were from GIBCO BRL Life Technologies, Inc. Commercial PTX injection was from Hainan Chuntch Pharmaceutical Co., Ltd. The other chemicals were analytical grade and from Sinopharm Chemical Reagent Co., Ltd.

2.2 Preparation of oleic acid modified Fe_3O_4 MNPs

Fe_3O_4 was synthesized using a co-precipitation method[30] with some modifications. Briefly, 12.5 g $FeCl_3·6H_2O$ and 7.5 g $FeSO_4·7H_2O$ were dissolved together in 25 mL deionized water in a three-necked flask. The solution was heated to 80 °C under nitrogen atmosphere. Subsequently, 25 mL $NH_3·H_2O$ (25%) and 2 g oleic acid were added into the solution. The
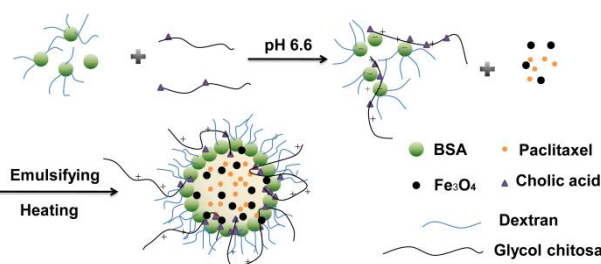
Scheme 1 Fabrication approach and structure of multifunctional Fe_3O_4/PTX@BD/GCCA emulsion.

mixture was reacted at 80 °C for 3 h. The produced oleic acid stabilized Fe_3O_4 MNPs were collected by an external magnetic field and washed with water repeatedly then suspended in hexane for purification. After centrifugation at 8000 rpm for 15 min to remove large particles, the purified Fe_3O_4 MNPs were precipitated using ethanol and then dried.

2.3 Synthesis and characterization of glycol chitosan-cholic acid (GCCA) conjugate

GCCA was synthesized by an amidation reaction between amine group of GCS and carboxyl group of CA as described in the literature.[31] Briefly, 500 mg GCS was dissolved in 50 mL deionized water and 0.2 mmol CA was dissolved in 50 mL methanol. Then, 0.3 mmol NHS and 0.3 mmol EDC were added into the methanol solution to activate the carboxyl group of CA for 30 min. The activated CA solution was dropwise added into the GCS solution. After 24 h reaction at 37 °C, the produced GCCA conjugate was purified by dialysis against a mixed solvent of CH_3OH and H_2O (1:1, v/v) and then against deionized water. The purified GCCA was obtained after lyophilization.

GCCA was characterized by FTIR (Nicolet 6700, Thermofisher) and ^{1}H-NMR (AVANCE III HD 400MHz, Bruker BioSpin International). For ^{1}H-NMR characterization, CA and GCS were separately dissolved in d_6-DMSO and D_2O, and GCCA was dissolved in a mixed solvent of D_2O and CD_3OD (1:1, v/v). The CA substitution degree, the average number of CA groups in per 100 sugar residues of GCS, was determined by colloidal titration in which the primary amine contents in GCCA and GCS samples were analyzed using potassium poly(vinyl sulfate) standard solution as titrant and toluidine blue as indicator.[31] Every sample was analyzed in triplicate and the average value was reported.

2.4 Preparation of BSA-dextran (BD) conjugate

BD was prepared by Maillard reaction as previously reported.[24] Briefly, the mixed aqueous solution of BSA and dextran with a molar ratio of BSA to dextran 1:6 was adjusted to pH 8.0 and then lyophilized. The lyophilized powder was reacted at 60 °C and 79% relative humidity for 48 h. The produced BD conjugate without purification was directly used in the following study. For the purpose of simplifying the description, only BSA concentration was presented to denote the BD concentration in this paper.

2.5 Preparation and characterization of Fe_3O_4 and PTX loaded BD/GCCA (Fe_3O_4/PTX@BD/GCCA) emulsion

BD and GCCA were dissolved together in deionized water and the solution was adjusted to desired pH value and then kept at room temperature for 4 h to allow the formation of BD/GCCA electrostatic complex. Fe_3O_4 and PTX were dispersed together in MCT containing 5% (v/v) ethanol by ultrasound. The PTX concentration in the oil solution was 8 mg mL^{-1}. The oil solution was added into the aqueous solution with a 20% oil volume fraction. The mixture was pre-emulsified using a homogenizer (FJ200-S, Shanghai Specimen Model Co.) at 10,000 rpm for 1 min, and immediately emulsified using a high pressure homogenizer (AH100D, ATS Engineering Inc.) at 800 bar for 4 min. The produced emulsion was adjusted to pH 7.8 and then heated at 90 °C for 1 h to form irreversible BSA interfacial films.[24] Similarly, BD/GCCA emulsion, PTX@BD/GCCA emulsion and Fe_3O_4@BD/GCCA emulsion were prepared.

Unloaded PTX in the emulsion was extracted by chloroform and analyzed on a HPLC system (2545 system; Waters Corp.). Fe concentration in the emulsion was analyzed on an inductively coupled plasma atomic emission spectrometer (ICP-AES, Hitachi P-4010). The ICP-AES samples were prepared as reported previously.[32] Z-average hydrodynamic diameter (D_h), polydispersity index (PDI) and ζ-potential of the droplets were measured using a Zetasizer Nano (ZS 90, Malvern Instruments). For D_h and PDI measurements, the emulsion was diluted 1000-fold with water. For ζ-potential measurement, the emulsion was diluted 1000-fold with the aqueous solution containing desired pH value and 5 mM NaCl. Transmission electron microscopy (TEM) observations of the droplets as well as Fe_3O_4 MNPs were conducted on a Philips CM120 electron microscope.

2.6 *In vivo* anti-tumor efficacy of the emulsions

The animal experiments on tumor therapy of this study were carried out at Experimental Animal Center of School of Pharmacy of Fudan University in full compliance with the guidelines approved by Shanghai Administration of Experimental Animals. Male ICR mice (SPF, 18–22 g) from Sino-British SIPPR/BK Lab. Animal Ltd. were inoculated in right armpit with H22 ascites. The mice were randomly assigned to five treatment groups with ten in each group. The treatment started after 3 days of the inoculation. Commercial PTX injection, PTX@BD/GCCA and Fe_3O_4/PTX@BD/GCCA emulsions were separately injected via the tail veins at PTX dose of 15 mg kg^{-1} after 3, 5, 6 and 8 days of the inoculation. Physiological saline and BD/GCCA emulsion were also administrated as controls. After each injection, each mouse in Fe_3O_4/PTX@BD/GCCA + Field group was immediately treated with an external magnetic field by binding a small magnet of 0.15 T to the tumor for 4 h. After 10 days of the inoculation, all the mice were sacrificed and the solid tumors were taken out and weighed. The tumor inhibition rate (*TIR*) was calculated according to the following equation: TIR (%) = $(1 - W_T/W_C) \times 100$ %, where W_T is the average tumor weight of the treated group and W_C is the average tumor weight of the saline group.

2.7 *In vitro* MRI and *in vivo* tumor MRI of the emulsions

Fe_3O_4/PTX@BD/GCCA emulsion with Fe concentration of 0.322 mg mL^{-1} and Fe_3O_4@BD/GCCA emulsion with Fe concentration of 0.257 mg mL^{-1} were diluted to different Fe concentrations with 1% agarose solution. Transverse relaxation time (T_2)-weighted magnetic resonance (MR) images of the samples were acquired using a clinical MRI instrument (Siemens 3T Trio MRI system). The parameters of T_2-weighted fast-recovery fast spin-echo (FR-FSE) sequence are as follows: TR 3000 ms, TE 39.6 ms, matrix size 640 × 640, slice thickness 5 mm, field of view (FOV) 128 × 128 mm^2. Transverse relaxation rates (R_2) of Fe_3O_4/PTX@BD/GCCA and Fe_3O_4@BD/GCCA were obtained by linear fitting of $1/T_2$ versus Fe concentration.

The animal experiments on MRI of this study were performed at Department of Laboratory Animal Science of Fudan University in complete compliance with the guidelines approved by Shanghai Administration of Experimental Animals. Male BALB/c nude mice (SPF, 20 g) were from Shanghai SLAC Lab. Animal Co., Ltd. MGC 803 solid tumors were implanted into the right hindquarters of the mice. After the tumors growing to about 500 mm^3, the nude mice were injected with 0.25 mL Fe_3O_4/PTX@BD/GCCA emulsion containing 0.45 mg mL^{-1} Fe concentration via tail veins. A small magnet of 0.15 T was bound to the tumor for 0, 1.5 and 12 h separately. Before being fixed in a stereotaxic apparatus for MRI on a 3T clinical MRI instrument with an animal coil, each mouse was anaesthetized by intraperitoneal injection with 10% chloral hydrate solution at a dose of 400 mg kg^{-1}. The parameters of FR-FSE sequence are as follows: TR 3500 ms, TE 76 ms, matrix size 256 × 256, slice thickness 0.8 mm, FOV 70 × 70 mm^2, number of acquisitions 8.

2.8 *In vitro* photothermal conversion and *in vivo* tumor phototherapy of the emulsions

Fe_3O_4@BD/GCCA emulsion of 0.1 mL with Fe concentration of 0.09, 0.22 or 0.45 mg mL^{-1} was exposed to an 808 nm laser (MDL-III-808-2.5W, Changchun New Industries Optoelectronics Technology Co., Ltd.) irradiation for 5 min at a power density of 5 W cm^{-2}. The emulsion temperature was measured every 60 s by a thermoelectric couple. The photothermal transduction efficiency of the emulsion was calculated as reported in the literature.[33]

Male ICR mice (25 g) were inoculated in right hindquarter with H22 ascites. After the tumors growing to about 100 mm^3, 0.1 mL of physiological saline, Fe_3O_4@BD/GCCA emulsion and Fe_3O_4/PTX@BD/GCCA emulsion with Fe concentration of 0.45 mg mL^{-1} were separately injected into the tumors. For the groups with NIR laser irradiation, each tumor was exposed to 808 nm laser at a power density of 5 W cm^{-2} for 10 min immediately after the injection. The tumor volumes were measured every other day using a caliper according to the method reported in the literature.[34]

3 Results and discussion

3.1 Synthesis and characterization of GCCA conjugate

In this study, we used GCCA and BD electrostatic complex as a complex emulsifier to produce Fe_3O_4 MNPs and PTX loaded
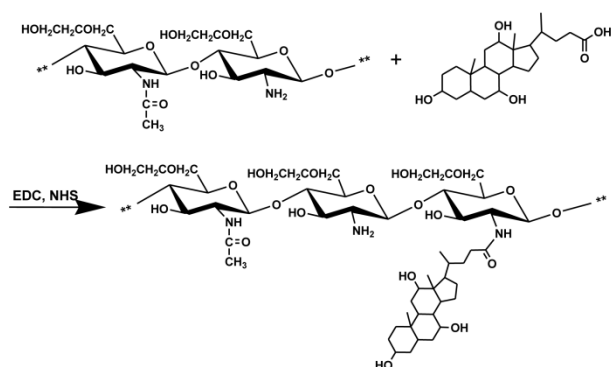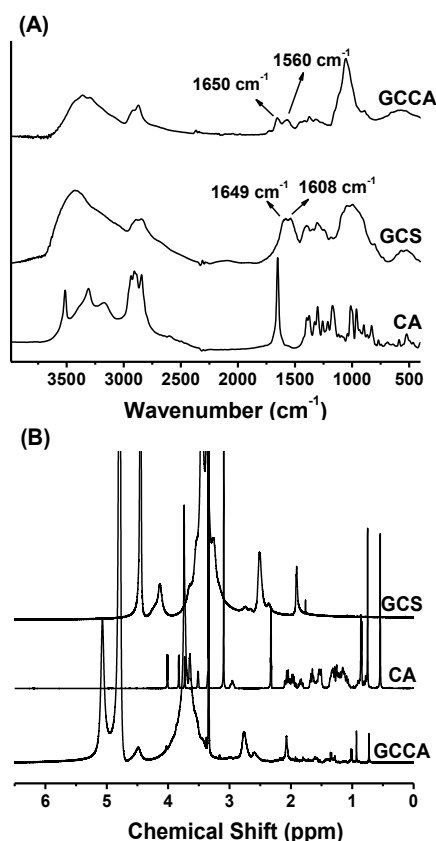
Scheme 2 Synthetic route and structure of GCCA.

Fig. 1 (A) FTIR spectra of GCS, CA and GCCA, and (B) ^{1}H NMR spectra of GCS (in D_2O), CA (in d_6-DMSO) and GCCA (in D_2O/CD_3OD).

emulsion for tumor diagnosis and therapy. GCCA was synthesized by an amidation reaction between the amine group of GCS and the carboxyl group of CA in the presence of EDC and NHS (Scheme 2). FTIR spectrum of GCS (Fig. 1A) presents the peaks at 1649 cm^{-1} (amide I, C=O stretching) and 1608 cm^{-1} (primary amine, N–H bending).[35] In GCCA spectrum, the peak at 1608 cm^{-1} weakens and the peak at 1560 cm^{-1} (amide II, N–H bending) appears, demonstrating the formation of amide bonds[36] between GCS and CA. This result is further verified by ^{1}H-NMR spectra shown in Fig. 1B. For ^{1}H-NMR characterization, GCCA was dissolved in a mixed solvent of D_2O and CD_3OD to avoid the hydrophobic aggregation of the CA groups. The peaks at 0.6–2.5 ppm in the GCCA spectrum correspond to the protons of CA groups,[37] indicating that CA

groups have been successfully grafted to GCS. The CA substitution degree in GCCA is 6.16($\pm$0.72)% determined by colloid titration; that is, each GCS chain, which contains 400 sugar residues, conjugated about 24.6 CA groups on average.

3.2 Preparation and characterization of BD/GCCA emulsion

BD conjugate was produced by Maillard reaction as previously reported[24] in which the reducing-end carbonyl group of dextran was conjugated to the amine group of BSA and no other chemical was needed. After the Maillard reaction, each BSA molecule conjugated about 4.4 dextran chains on average. Previously, we used BD as an emulsifier to produce stable emulsion with BSA oil-water interfacial film and dextran surface. The dextran surface enables the oil droplets to be dispersible in aqueous solution and also endows the droplets with a "stealth" property to avoid reticuloendothelial recognition and subsequent elimination.[24,38] In this study, we intended to produce stable emulsion with pH sensitive charge-conversional surface. Amphiphilic GCCA possesses surface activity. Hydrophobic CA groups enter into oil phase and hydrophilic GCS chains are on the droplet surface. However, polysaccharide emulsion, whose droplets are much larger than those of BD emulsion, is not stable.[19,39,40] Herein, we used BD/GCCA electrostatic complex as a complex emulsifier to fabricate stable emulsion with pH sensitive charge-conversional surface.

In the pH range of 5.0–8.0, GCCA presents similar positive ζ-potentials as GCS (Fig. 2A), whereas BD is negatively charged, suggesting that BD and GCCA can form electrostatic complex in this pH range. To optimize the pH condition, GCCA and BD mixed aqueous solution containing 0.5 mg mL^{-1} GCCA and 7.5 mg mL^{-1} BSA was adjusted to different pH values, and then MCT was added to reach 20% volume fraction for emulsification. After emulsification, the emulsions were heated at 90 °C for 1 h to induce BSA gelation thus to form irreversible oil-water interfacial films, which can avoid the coalescence of the oil droplets and also eliminate BSA anaphylaxis.[24] Subsequently, the emulsions were adjusted to pH 5.0 and 7.4 to investigate the pH sensitive charge-conversion property. Fig. 2B shows that the BD/GCCA emulsions produced in the pH range of 5.5–7.5 possess similar ζ-potentials at pH 5.0 as well as at pH 7.4, suggesting that these emulsions have similar surface structure. Relatively, the BD/GCCA emulsion produced at pH 6.6 has a smaller D_h value, indicating that the emulsifying ability of the complex at pH 6.6 is better. Therefore, we adopted pH 6.6 as the emulsification pH condition in the following study.

The influence of GCCA concentration on the BD/GCCA emulsions was investigated. The D_h, PDI and ζ-potential of the droplets increase respectively when changing the GCCA concentration from 0 to 1 mg mL^{-1} and fixing the BSA concentration at 7.5 mg mL^{-1} (Fig. 2C). More GCCA molecules in the complex lead the droplet surface to possess more positive charges at acidic pH condition. On the other hand, more GCCA molecules result in the emulsion unstable. In the following study, we used 0.5 mg mL^{-1} GCCA concentration to produce BD/GCCA emulsion. At this GCCA concentration the
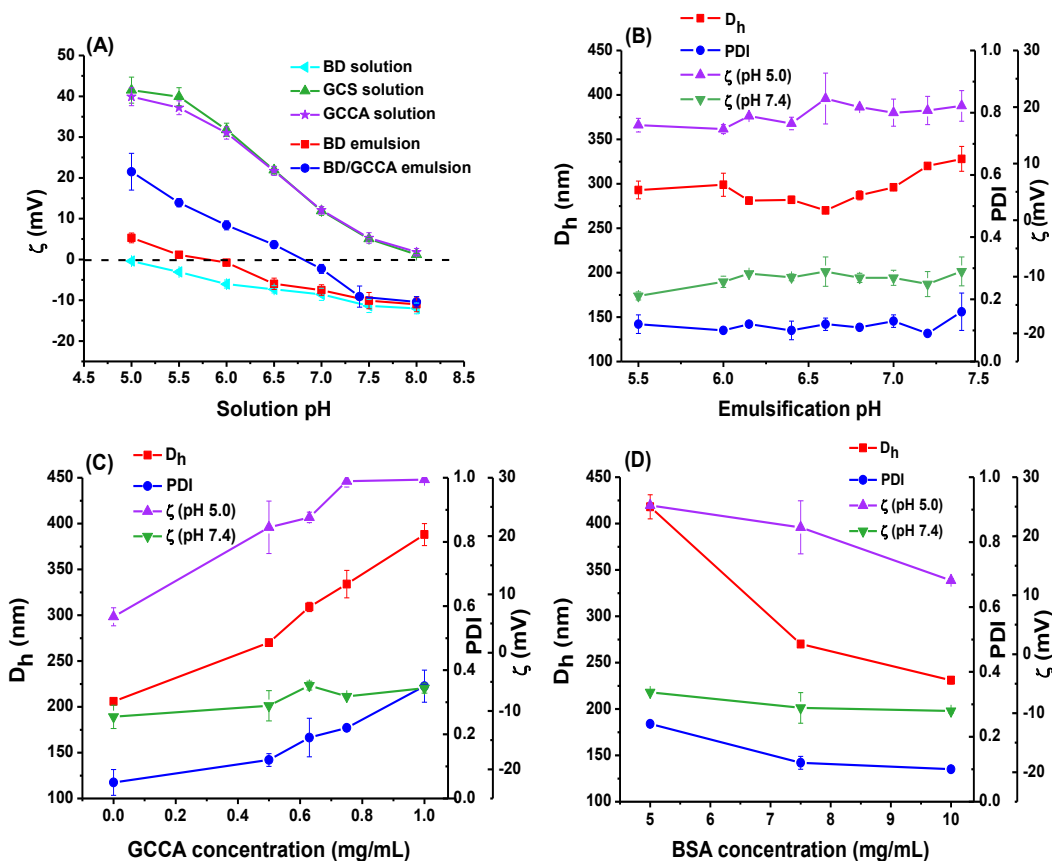
COMMUNICATION

Fig. 2 (A) pH dependent ζ-potentials of GCS, GCCA and BD solutions, as well as BD and BD/GCCA emulsions produced at optimized condition; droplet size, PDI and ζ-potentials of the BD/GCCA emulsions produced at (B) different emulsification pH conditions, (C) different GCCA concentrations and (D) different BSA concentrations.

Table 1 Loading efficiency (LE) of PTX in Fe_3O_4/PTX@BD/GCCA emulsions with and without 5% ethanol in MCT, and storage stability of the emulsions at pH 7.4 and 5.0 and 4 ^oC.

V_{EtOH}/V_{MCT}	Storage time (day)	pH 7.4		pH 5.0		LE (%)
		D_h (nm)	PDI	D_h (nm)	PDI	
0	0	270 ±2	0.16 ±0.02	266 ±4	0.18 ±0.02	92.4
	14	269 ±12	0.14 ±0.01	262 ±1	0.15 ±0.01	
1:19	0	251 ±4	0.16 ±0.01	257 ±12	0.17 ±0.02	95.4
	14	273 ±1	0.20 ±0.01	254 ±13	0.15 ±0.01	

droplet size does not increase much but the ζ-potential at pH 5.0 increases significantly compared with the emulsion without GCCA. The influence of BD concentration on the BD/GCCA emulsions was also investigated. When changing the BSA concentration from 5 to 10 mg mL^{-1}, the D_h, PDI and positive charges of the droplets decrease gradually (Fig. 2D). Considering both D_h and surface charges, the BSA concentration was fixed at 7.5 mg mL^{-1} in the following study.

Fig. 2A verifies that the BD/GCCA emulsion produced at optimal condition, 0.5 mg mL^{-1} GCCA and 7.5 mg mL^{-1} BSA in pH 6.6 aqueous solution and 20% oil volume fraction, possesses pH sensitive charge-conversion property. The droplets are positively charged at pH 6.5 and negatively charged at pH 7.4. This property can increase the tumorous cellular uptake meanwhile prolong the blood circulation time of the droplets.
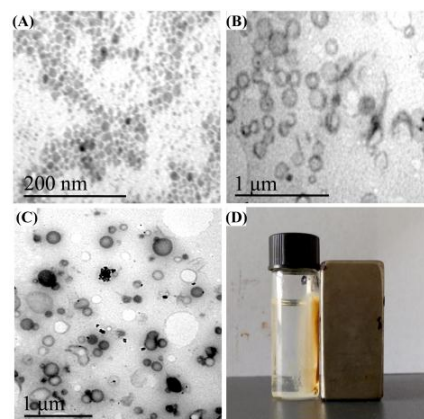

Fig. 3 TEM images of (A) oleic acid modified Fe_3O_4 MNPs, (B) PTX@BD/GCCA emulsion and (C) Fe_3O_4/PTX@BD/GCCA emulsion; (D) photo of Fe_3O_4/PTX@BD/GCCA emulsion under an external magnetic field after 10-fold dilution with deionized water.

Table 2 Storage stability of Fe$_3$O$_4$/PTX@BD/GCCA emulsion after 10-fold dilution with DMEM cell culture medium containing 10% fetal bovine serum.

Storage time (day)	D$_h$ (nm)	PDI
0	248 ±1	0.20 ±0.01
21	246 ±2	0.16 ±0.03

3.3 Preparation and characterization of Fe$_3$O$_4$/PTX@BD/GCCA emulsion

Fig. 3A shows that the diameters of oleic acid modified Fe$_3$O$_4$ MNPs are about 8−20 nm. Hydrophobic PTX and MNPs were dispersed in MCT containing 5% ethanol which can increase the solubility of PTX in MCT and also can penetrate into surfactant layer to improve emulsifying property.[41] The data in Table 1 show that the droplet size of freshly prepared Fe$_3$O$_4$/PTX@BD/GCCA emulsion decreases from 270 to 251 nm, and the loading efficiency of PTX in the emulsion increases from 92.4% to 95.4% after addition of 5% ethanol in MCT phase. Fig. 3B and 3C show the TEM images of PTX@BD/GCCA and Fe$_3$O$_4$/PTX@BD/GCCA droplets, respectively; the droplets present an integrated periphery. Fig. 3D shows the magnetic response property of Fe$_3$O$_4$/PTX@BD/GCCA emulsion after 10-fold dilution. The Fe$_3$O$_4$/PTX@BD/GCCA droplets were completely aggregated after applying an external magnetic field for 12 h. After the aggregation under magnetic field, the emulsion became transparent, suggesting that almost all the droplets contain MNPs and have excellent magnetic responsiveness.

After preparation, Fe$_3$O$_4$/PTX@BD/GCCA emulsion was adjusted to pH 5.0 or pH 7.4 and then stored at 4 °C to investigate the stability. Table 1 shows that the emulsions with and without ethanol in MCT do not change significantly in droplet size and PDI after 14 days of storage at both pH 5.0 and 7.4. Furthermore, Fe$_3$O$_4$/PTX@BD/GCCA emulsion also shows good stability after 10-fold dilution with DMEM cell culture medium containing 10% fetal bovine serum. The droplet size and PDI do not change significantly after 21 days of the storage as shown in Table 2, indicating that Fe$_3$O$_4$/PTX@BD/GCCA emulsion is long-term stable at physiological environment. In Fe$_3$O$_4$/PTX@BD/GC emulsion, hydrophobic CA groups enter into oil phase,[42] amphiphilic BSA locates at oil-water interface,[24] and hydrophilic dextran and GCS on the droplet surface extend in the aqueous phase that make the droplets stable.
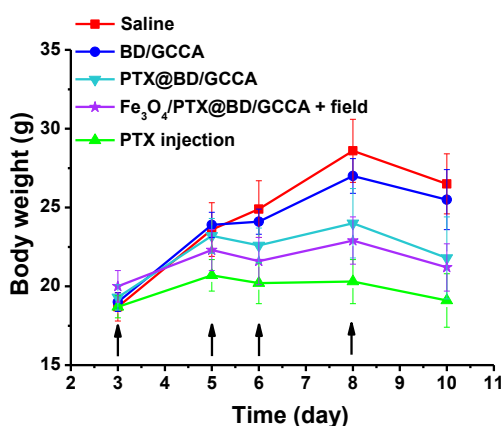
Fig. 4 Average body weight changes of H22 tumor-bearing mice during the various treatments. The arrows indicate the days when the treatments performed.

3.4 *In vivo* anti-tumor efficacy of the emulsions

In vivo anti-tumor efficacy of multifunctional Fe$_3$O$_4$/PTX@BD/GCCA emulsion was evaluated by H22 tumor-bearing mice. The mice were treated with PTX dose of 15 mg kg^{-1} via the tail veins after 3, 5, 6 and 8 days of the inoculation. The tumor inhibition rates of the various treatment groups are shown in Table 3. BD/GCCA emulsion, the equivalent empty carrier, has no significant anti-tumor activity compared with physiological saline. The average body weights of BD/GCCA group during the treatment are closed to the weights of physiological saline group as shown in Fig. 4 indicating that BD/GCCA emulsion does not have toxicity significantly. The tumor inhibition rate of PTX@BD/GCCA group is 50.0%, which is only slightly higher than the rate of commercial PTX injection group (Table 3). However, no mice died during the treatment in PTX@BD/GCCA group, whereas two mice died in commercial PTX injection group. This result demonstrates that the toxicity of PTX@BD/GCCA emulsion is lower than the toxicity of commercial PTX injection. The average body weights shown in Fig. 4 also confirm that PTX@BD/GCCA emulsion is more biocompatible than commercial PTX injection. For Fe$_3$O$_4$/PTX@BD/GCCA group with an external magnetic field, the tumor inhibition rate is 68.3%, significantly higher than 47.0% of commercial PTX injection group. During the treatment, no mice died (Table 3), and the average body weights of Fe$_3$O$_4$/PTX@BD/GCCA group are higher than the weights of commercial PTX injection

Table 3 H22 tumor inhibition effects of the emulsions with and without an external magnetic field.

Group	Mice number (beginning/end)	Average tumor weight (g)	Tumor inhibition rate (%)
Physiological saline	10/10	1.64 ±0.26	/
BD/GCCA	10/10	1.36 ±0.17	/
PTX injection	10/8	0.87 ±0.21[a]	47.0
PTX@BD/GCCA	10/10	0.82 ±0.30 [a,b]	50.0
Fe$_3$O$_4$/PTX@BD/GCCA + field	10/10	0.52 ±0.27 [a,c,d]	68.3

[a] $P < 0.001$ compared with physiological saline group; [b] $P > 0.05$ compared with commercial PTX injection group; [c] $P < 0.01$ compared with commercial PTX injection group; [d] $P < 0.05$ compared with PTX@BD/GCCA group.
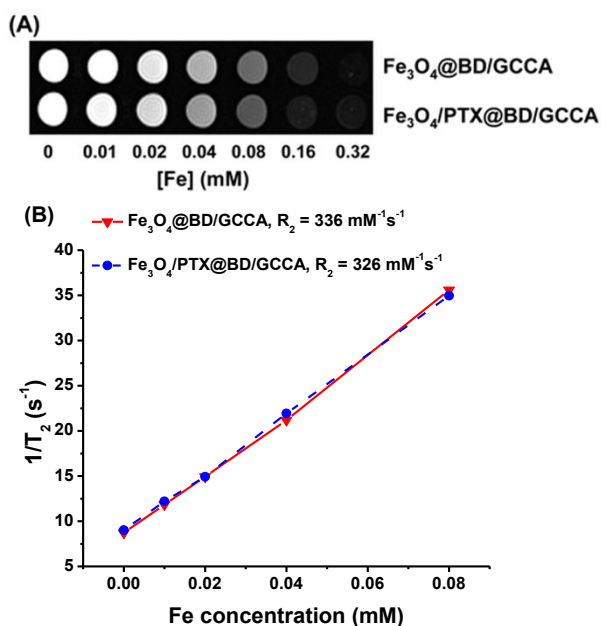
Fig. 5 (A) T_2-weighted MR images of Fe$_3$O$_4$@BD/GCCA and Fe$_3$O$_4$/PTX@BD/GCCA emulsions after dilution and suspension in 1% agarose hydrogel; (B) 1/T_2 changes of the emulsions as a function of Fe concentration.
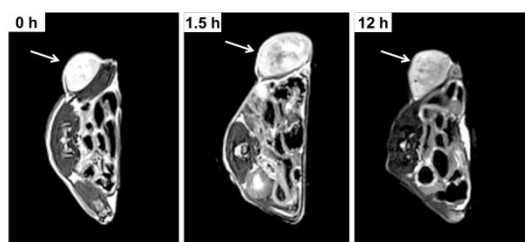

Fig. 6 MR images of MGC 803 tumor-bearing nude mice acquired at 0, 1.5 and 12 h post-injection of Fe$_3$O$_4$/PTX@BD/GCCA emulsion with magnetic targeting. White arrow indicates tumor.

group (Fig. 4). These results can be explained by the fact that Fe$_3$O$_4$/PTX@BD/GCCA droplets can be effectively accumulated at tumor site when attaching a small magnet to the tumor. Furthermore, it is possible that the accumulated droplets can be internalized by tumor tissue due to the charge-conversion property of the emulsion. Therefore, Fe$_3$O$_4$/PTX@BD/GCCA emulsion can significantly enhance the anti-tumor efficacy meanwhile reduce the toxicity of PTX.

3.5 *In vitro* MRI and *in vivo* tumor MRI of the emulsions

Fe$_3$O$_4$ MNPs can be used as T_2-imaging contrast agents which generate dark contrast in MRI.[43] After dilution and suspension in 1% agarose hydrogel, the T_2-weighted images of Fe$_3$O$_4$@BD/GCCA and Fe$_3$O$_4$/PTX@BD/GCCA emulsions were acquired. Fig. 5A shows that the MRI signal intensities of the emulsions decrease gradually with the increase of Fe concentration. The R_2 relaxation rates were calculated through the linear fitting of 1/T_2 versus Fe concentration (Fig. 5B). The R_2 values of Fe$_3$O$_4$@BD/GCCA and Fe$_3$O$_4$/PTX@BD/GCCA emulsions are 336 mM^{-1}s^{-1} and 326 mM^{-1}s^{-1}, respectively, which are much higher than the R_2 value of 123 mM^{-1}s^{-1} of Feridex, a commercial T_2-weighted contrast agent.[44] The much higher R_2 values indicate that
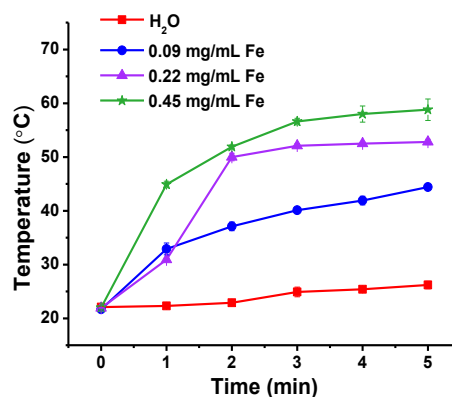

Fig. 7 Temperature changes of Fe$_3$O$_4$/PTX@BD/GCCA emulsions with different Fe concentrations after NIR laser irradiation at a power density of 5 W cm^{-2}.
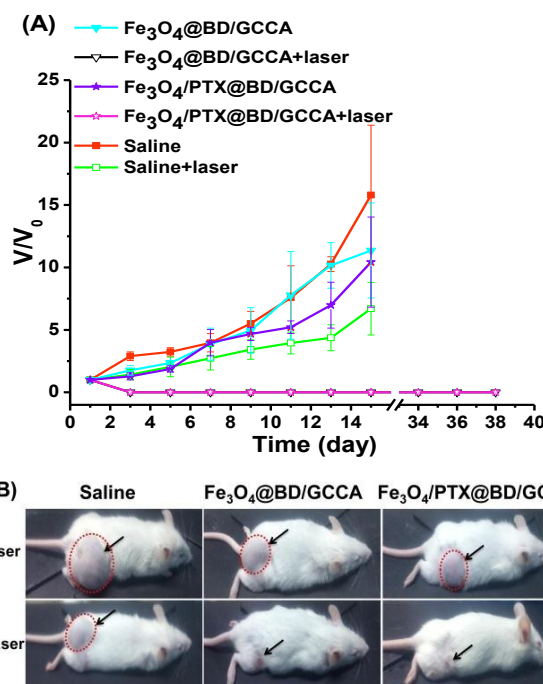

Fig. 8 (A) Relative average tumor volume changes of six treatment groups (n = 5) after the treatment of intratumoral injection and NIR irradiation, and (B) photos of the mice taken at 19 day post-injection and irradiation. Tumors are indicated by arrows and dashed lines.

Fe$_3$O$_4$@BD/GCCA and Fe$_3$O$_4$/PTX@BD/GCCA emulsions can generate better T_2 contrast in MRI.

Fe$_3$O$_4$/PTX@BD/GCCA emulsion with Fe concentration of 0.45 mg mL^{-1} was injected into MGC 803 tumor-bearing nude mice via tail veins, and a magnet of 0.15 T was immediately bound to the tumor after the injection. After 0, 1.5 and 12 h post-injection, T_2-weighted MR images of tumors were acquired *in vivo*. The image acquired at 1.5 h post-injection presents better contrast effect than the image taken at 0 h post-injection, and the effect further improves in the image acquired at 12 h post-injection (Fig. 6). This result confirms that the Fe$_3$O$_4$/PTX@BD/GCCA concentration in the tumor tissue increased from 0 to 12 h when guided by an external magnetic field. Considering the anti-tumor efficacy (Table 1) and the contrast effect in MRI (Fig. 6), Fe$_3$O$_4$/PTX@BD/GCCA

COMMUNICATION

Journal Name

emulsion may have a potential to be used synchronously for tumor therapy and MRI.

3.6 *In vitro* photothermal conversion and *in vivo* tumor phototherapy of the emulsions

In vitro photothermal conversion effect of Fe_3O_4/PTX@BD/GCCA was evaluated by exposing the emulsions with Fe concentrations of 0.09, 0.22 and 0.45 mg mL^{-1} to an 808 nm laser at a power density of 5 W cm^{-2}. Fig. 7 shows the temperatures of the emulsions during the irradiation. Compared with deionized water, the emulsions have remarkable photothermal conversion effect. The effect enhances when increasing Fe concentration in the emulsion. For the emulsion with 0.45 mg mL^{-1} Fe concentration, the temperature ascended from 22 to 45 °C after 1 min irradiation and to 59 °C after 5 min irradiation; the photothermal transduction efficiency is 10.1%.

In vivo tumor phototherapy of Fe_3O_4@BD/GCCA and Fe_3O_4/PTX@BD/GCCA emulsions was evaluated by H22 tumor-bearing mice. The treatment was performed by a single intratumoral injection of 0.1 mL emulsion with Fe concentration of 0.45 mg mL^{-1}. For the groups with NIR laser irradiation, the tumor was exposed to 808 nm laser at a power density of 5 W cm^{-2} for 10 min immediately after the injection. Fig. 8A shows the efficacy of photothermal therapy. All the tumors in Fe_3O_4@BD/GCCA + laser group and Fe_3O_4/PTX@BD/GCCA + laser group disappeared completely within two days and did not appear any more, whereas the tumors in other groups grew faster and faster and death occurred after 16 days of the treatment. For saline + laser group, the tumors are significantly smaller than those of saline group without irradiation. This result suggests that only NIR irradiation has some effect on tumor inhibition but cannot eliminate tumor. In addition, the tumors in Fe_3O_4/PTX@BD/GCCA group are smaller than the tumors in Fe_3O_4@BD/GCCA group due to the pesticide effect of PTX. Fig. 8B presents the photos of the mice from the six treatment groups after 19 days of the treatment for visualization. In Fe_3O_4@BD/GCCA + laser group and Fe_3O_4/PTX@BD/GCCA + laser group, no tumor appeared and no mouse died even after 38 days of the treatment. It looks that all the tumors in these groups have been cured. The result in Fig. 8 demonstrates that Fe_3O_4@BD/GCCA and Fe_3O_4/PTX@BD/GCCA emulsions can completely eliminate tumor via intratumoral injection and NIR thermotherapy.

4 Conclusions

In this study, we used BD/GCCA electrostatic complex as emulsifier to fabricate Fe_3O_4/PTX@BD/GCCA emulsion for tumor-targeted chemotherapy, MRI and NIR photothermal therapy. The fabrication of Fe_3O_4/PTX@BD/GCCA emulsion is simple and high efficient. The emulsion is stable at physiological condition. The droplet surfaces are negatively charged at pH 7.4 and positively charged at pH 6.5. Fe_3O_4/PTX@BD/GCCA droplets can be effectively accumulated at tumor site by attaching a small magnet to

tumor and the pH sensitive charge-conversional surfaces may promote the tumorous cellular uptake of the droplets. The emulsion significantly enhanced the anti-tumor efficacy and reduced the toxicity of PTX as well as improved the tumor contrast effect in T_2-weighted MRI after administration via tail vein and applying an external magnetic field to the tumor. Furthermore, it is notable that the emulsion can completely eliminate tumor after intratumoral injection and NIR laser irradiation. This study demonstrates that Fe_3O_4/PTX@BD/GCCA emulsion, which does not need special receptor recognition, is a promising system for tumor diagnosis and therapy.

Notes and references

1 A. Singh and S. K. Sahoo, *Drug Discov. Today*, 2014, **19**, 474-481.
2 A. J. Cole, V. C. Yang and A. E. David, *Trends Biotechnol.*, 2011, **29**, 323-332.
3 J. Xie, G. Liu, H. S. Eden, H. Ai and X. Chen, *Accounts Chem. Res.*, 2011, **44**, 883-892.
4 Y. Zhao, Z. Qiu and J. Huang, *Chin. J. Chem. Eng.*, 2008, **16**, 451-455.
5 J. Qu, H. Shao, G. Jing and F. Huang, *Colloid Surf., B*, 2013, **102**, 37-44.
6 M. Chu, Y. Shao, J. Peng, X. Dai, H. Li, Q. Wu and D. Shi, *Biomaterials*, 2013, **34**, 4078-4088.
7 N. Ahmed, H. Fessi and A. Elaissari, *Drug Discov. Today*, 2012, **17**, 928-934.
8 N. Schleich, F. Danhier and V. Préat, *J. Controlled Release*, 2015, **198**, 35-54.
9 X. Zhao, Z. Chen, H. Zhao, D. Zhang, L. Tao and M. Lan, *RSC Adv.*, 2014, **4**, 62153-62159.
10 S. Shen, F. Kong, X. Guo, L. Wu, H. Shen, M. Xie, X. Wang, Y. Jin and Y. Ge, *Nanoscale*, 2013, **5**, 8056-8066.
11 Z. Zhou, Y. Sun, J. Shen, J. Wei, C. Yu, B. Kong, W. Liu, H. Yang, S. Yang and W. Wang, *Biomaterials*, 2014, **35**, 7470-7478.
12 H. Chen, C. Khemtong, X. Yang, X. Chang and J. Gao, *Drug Discov. Today*, 2011, **16**, 354-360.
13 A. Wicki, D. Witzigmann, V. Balasubramanian and J. Huwyler, *J. Controlled Release*, 2015, **200**, 138-157.
14 F. Jia, X. Liu, L. Li, S. Mallapragada, B. Narasimhan and Q. Wang, *J. Controlled Release*, 2013, **172**, 1020-1034.
15 Z. Ahmad, A. Shah, M. Siddiq and H. Kraatz, *RSC Adv.*, 2014, **4**, 17028-17038.
16 E. B. Souto, A. P. Nayak and R. S. R. Murthy, *Pharmazie*, 2011, **66**, 473-478.
17 N. K. Ibrahim, N. Desai, S. Legha, P. Soon-Shiong, R. L. Theriault, E. Rivera, B. Esmaeli, S. E. Ring, A. Bedikian, G. N. Hortobagyi and J. A. Ellerhorst, *Clin. Cancer Res.*, 2002, **8**, 1038-1044.
18 A. Maali and M. T. H. Mosavian, *J. Dispersion Sci. Technol.*, 2013, **34**, 92-105.
19 E. Bouyer, G. Mekhloufi, V. Rosilio, J. Grossiord and F. Agnely, *Int. J. Pharm.*, 2012, **436**, 359-378.

20 P. A. Kramer, *J. Pharm. Sci.*, 1974, **63**, 1646-1647.
21 M. J. Hawkins, P. Soon-Shiong and N. Desai, *Adv. Drug Deliv. Rev.*, 2008, **60**, 876-885.
22 B. Zeeb, H. Zhang, M. Gibis, L. Fischer and J. Weiss, *Food Res. Int.*, 2013, **53**, 325-333.
23 M. Evans, I. Ratcliffe and P. A. Williams, *Curr. Opin. Colloid Interface Sci.*, 2013, **18**, 272-282.
24 J. Qi, C. Huang, F. He and P. Yao, *J. Pharm. Sci.*, 2013, **102**, 1307-1317.
25 Z. Yue, W. Wei, P. Lv, H. Yue, L. Wang, Z. Su and G. Ma, *Biomacromolecules*, 2011, **12**, 2440-2446.
26 C. He, Y. Hu, L. Yin, C. Tang and C. Yin, *Biomaterials*, 2010, **31**, 3657-3666.
27 S. Honary and F. Zahir, *Trop. J. Pharm. Res.*, 2013, **12**. 265-273.
28 J. Yu, H. Deng, F. Xie, W. Chen, B. Zhu and Q. Xu, *Biomaterials*, 2014, **35**, 3132-3144.
29 J. Kim, Y. Kim, S. Kim, J. H. Park, K. Kim, K. Choi, H. Chung, S. Y. Jeong, R. Park, I. Kim and I. C. Kwon, *J. Controlled Release*, 2006, **111**, 228-234.
30 P. C. Papaphilippou, A. Pourgouris, O. Marinica, A. Taculescu, G. I. Athanasopoulos, L. Vekas and T. Krasia-Christoforou, *J. Magn. Magn. Mater.*, **2011**, 323, 557-563.
31 S. Kwon, J. H. Park, H. Chung, I. C. Kwon, S. Y. Jeong and I. Kim, *Langmuir*, 2003, **19**, 10188-10193.
32 H. Hao, Q. Ma, F. He and P. Yao, *J. Mat. Chem. B*, 2014, **2**, 7978-7987.
33 C. M. Hessel, V. P. Pattani, M. Rasch, M. G. Panthani, B. Koo, J. W. Tunnell and B. A. Korgel, *Nano lett.*, 2011, **11**, 2560-2566.
34 T. Li, C. Huang, P. Ruan, K. Chuang, K. Huang, D. Shieh and C Yeh, *Biomaterials*, 2013, **34**, 7873-7883.
35 Z. Liu and P. Yao, *Polym. Chem.*, 2014, **5**, 1072-1081.
36 J. Yu, Y. Li, L. Qiu and Y. Jin, *Eur. Polym. J.*, 2008, **44**, 555-565.
37 K. Kim, S. Kwon, J. H. Park, H. Chung, S. Y. Jeong, I. C. Kwon and I. Kim, *Biomacromolecules*, 2005, **6**, 1154-1158.
38 H. Hao and P. Yao, *Chem. J. Chin. Univ.-Chin.*, 2014, **35**, 652-659.
39 M. S. Rodriguez, L. A. Albertengo and E. Agullo, *Carbohydr. Polym.*, 2002, **48**, 271-276.
40 U. Klinkesorn, *Food Rev. Int.*, 2013, **29**, 371-393.
41 A. A. Date and M. S. Nagarsenker, *Int. J. Pharm.*, 2008, **355**, 19-30.
42 T. Ngawhirunpat, N. Wonglertnirant, P. Opanasopit, U. Ruktanonchai, R. Yoksan, K. Wasanasuk and S. Chirachanchai, *Colloids Surf., B*, 2009, **74**, 253-259.
43 R. Thomas, I. Park and Y. Jeong, *Int. J. Mol. Sci.*, 2013, **14**. 15910-15930.
44 J. Xie, K. Chen, J. Huang, S. Lee, J. Wang, J. Gao, X. Li and X. Chen, *Biomaterials*, 2010, **31**, 3016-3022.

RSC Advances Accepted Manuscript